Electronic Supplement 8

Fire detection algorithms, 1985–1995

The 1980s saw a number of studies that used AVHRR MIR (band 3) data to detect, track and measure the spatial and temporal occurrence of natural (wild) fires and anthropogenic hot spots, i.e., those associated with oil platforms and industry. In her review, *Fire from space: Global fire evaluation using infrared remote sensing*, Robinson (1991) listed 14 papers that focused on such efforts using AVHRR data between 1980 and 1989, to which a 15th can be added: the study of Dozier (1980) (Table S8.1). In addition, two studies showed how SWIR data collected by Landsat's Thematic Mapper could be used to detect the hot spot associated with the April 1986 accident at the Chernobyl nuclear power plant (Richter *et al*., 1986), and to estimate its temperature and size (Rothery, 1989). Later studies showed how TM TIR data could be used to detect underground fires at coal mines (Prakash *et al*., 1995), and to estimate the associated ground temperature and fire depth (Saraf *et al*., 1995). In addition, using images acquired during the first gulf war, studies showed how AVHRR and TM data in both the VIS and TIR could be used to detect fires and to map their associated smoke plumes (Al-Hinai, 1991; Khazenie and Richardson, 1993; Stephens and Matson, 1993), with Meteosat VIS data being used to confirm model-based predictions for the extent of smoke plumes from burning oil wells in Kuwait (Bakan *et al*., 1991). Later studies also used AVHRR VIS and TIR data to assess and map fire risk on the basis of vegetation dryness (e.g., Paltridge and Barber, 1988; Vidal *et al*., 1994).

As part of these efforts, the decade spanning 1985 to 1995 saw the development of a number of algorithms to detect wild fires in AVHRR, as well as GOES-Imager, data, with Table S8.1 flagging the paper of Flannigan and Vonder Haar (1986), *Forest fire monitoring using NOAA satellite AVHRR*, as the first publication of an automated fire detection algorithm. In Table 5.2 of Chapter 5 I tabulated 11 different fire detection algorithms developed during these ten years. As indicated in Table 5.2, seven of these algorithms were fixed threshold. The remaining four were contextual, and included the first algorithm published: that of Flannigan and Vonder Haar (1986). These fire detection algorithms, and their physical basis, underpinned many of the volcanic hot spot detection algorithms that followed, and so are reviewed here.

Table S8.1. *Brief details of AVHRR fire studies as reviewed by Robinson (1991) [modified from Table 4 of Robinson (1991)].*

Study	Details	Reference
Dozier (1980)	Specifications of algorithms to estimate the size and temperature of sub-pixel hot spots using two bands of infrared (AVHRR) data (i.e., definition of the "dual-band method" of Chapter 4). Atmospheric correction methods also considered.	*NOAA Technical Memorandum*, **NOAA-81021710**, Washington, DC
Dozier (1981)	*Ditto*	*Remote Sensing of Environment*, **11**, 221–229.
Matson & Dozier (1981)	The Dozier (1980; 1981) algorithm applied to subpixel hot spots associated with oil flares in the Persian Gulf. Industrial hot spots around Detroit identified.	*Photogrammetric Engineering & Remote Sensing*, **47**, 1311–1318.
Wan (1985)	Simulation of smoke interference with fire signal reception using multiple scattering radiative transfer model linked to model of AVHRR response.	*PhD Dissertation*, University of Santa Barbara (CA).
Matson *et al.* (1984)	Case study of LAC fire imagery described for various sites; fire sightings in western U.S. compared to hot spots appearing in nighttime (2 am) HRPT images.	*NOAA Technical Report*, **NESDIS 7**, Washington, DC.
Muirhead & Cracknell (1984)	Rectification accuracy tested by comparing hot spot locations on rectified LAC (channel 3) images containing gas flare locations of known location and associated with North Sea drilling rigs.	*International Journal of Remote Sensing*, **5**, 199–212.
Muirhead & Cracknell (1985)	Hot spots counted on three rectified LAC channel 3 images of U.K. to assess straw burning and extent of compliance with bans on burning on certain days.	*International Journal of Remote Sensing*, **6**, 827–833.
Malingreau *et al.* (1985)	Hot spot chronology and NDVI studied across Borneo and E. Kalimantan during immense fires of 1983.	*Ambio*, **14**, 314–315.

Table S8.1. (*cont.*)

Study	Details	Reference
Malingreau (1984)	*Ditto*	*8th International Symposium on Remote Sensing of Environment*, held in Paris (France), 1–4 October 1984. Ann Arbor: Environmental Research Institute of Michigan.
Flannigan (1985)	Fire reports from severe fire outbreak in Alberta compared to fires detected by AVHRR. Dual-band algorithm used to estimate fire size and temperature. Cloud screening applied to reject cloud contaminated pixels.	*MSc. Thesis*, Colorado State University, Fort Collins (Colorado).
Flannigan & Vonder Haar (1986)	*Ditto*	*Canadian Journal of Forest Research*, **16**, 975–982.
Matson & Holben (1987)	Hot spots and vegetation studied on one LAC image for a 3 × 6 ° box over Manaus, Brazil. Dual-band algorithm applied.	*International Journal of Remote Sensing*, **8**, 509–516.
Malingreau & Tucker (1987)	Fire points in Southern Amazon Basin studied on a daily basis over two years in conjunction with studies of NDVI. Inference drawn about penetration of settlement into remote areas.	*Proceedings of IGARSS '87* held in Ann Arbor, Michigan, 18–21 May 1987. IEEE 87CH2434–9 (New York: IEEE), pp. 484–489.
Pereira (1988)	Fire counts and analysis of smoke trajectories with estimates of areas burned and mass combusted based on Brazilian HRPT data of Amazonia. Landsat TM compared to AVHRR.	INPE-4503-tdl/325, Inst. Nactional de Pesquisas Espacias, 12.201 Sao Jose dos Campos, SP, Brazil.
Setzer *et al*. (1988)	*Ditto*	INPE-4534-RPE/565, Inst. Nactional de Pesquisas Espacias, 12.201 Sao Jose dos Campos, SP, Brazil.

Acronyms:
HRPT: High Resolution Picture Transmission (direct read-out of AVHRR data to ground stations).
GAC: Global Area Coverage.
LAC: Local Area Coverage.
NDVI: Normalized Difference Vegetation Index
[see Cracknell (1997) for full definition of GAC + LAC data format]

Fixed threshold algorithms applied for fire detection: 1985–1995

Fixed threshold tests designed to detect fire-related hot spots in satellite data developed by the fire community between 1985–1995 tended to use MIR and TIR data to determine whether a pixel was hot or not. Plus, occasionally, VIS and NIR data to determine whether there were cloud or reflection problems. As detailed in Chapter 5, up to five fixed threshold tests could be applied to determine:

(1) Was the pixel hot?
(2) Was the pixel hot due to solar heating?
(3) Was there cloud contamination?
(4) Were there high levels of reflection?

Note, here, that the last two tests were designed to determine whether anomalously high brightness temperatures in the MIR, and hence also elevated ΔT (see Chapter 5 for definition and use), were due to high levels of reflection in the MIR. The pixel would have to pass all tests to be flagged as a fire pixel, and to then be used for fire counting or area mapping.

Generally tested on AVHRR data (all but one of the algorithms listed in Table 5.2 are designed to run on AVHRR), the algorithms also had to work with relatively low saturation levels (50 to 70 °C), so that most (if not all) fire-related hot spots tended to saturate the MIR. Solar heated and highly reflective surfaces could also saturate AVHRR's MIR band (see Electronic Supplement 1). Sunglint from water (ocean and lake) surfaces, for example, has frequently been observed to cause saturation of AVHRR band 3.

Kaufman et al. (1990)

The first fixed threshold algorithm for hot spot detection in satellite data was that of Kaufman *et al* (1990). Designed to run on AVHRR data to detect forest burning in Brazil, it was later applied by Kennedy *et al*. (1994) for fire detection in AVHRR data for West Africa. Using AVHRR channel 3 and 4 brightness temperature data (T_{MIR} and T_{TIR}), the algorithm applied three tests:

$$\begin{aligned} T_{MIR} &\geq 316\ \mathrm{K} \\ \Delta T &> 10\ \mathrm{K} \\ T_{TIR} &> 250\ \mathrm{K} \quad \text{(cloud test)} \end{aligned}$$

where ΔT was equal to T_{MIR}-T_{TIR}. The first test was designed to determine whether the pixel was close to saturation (i.e., greater that or equal to 43 °C, this being within 4 °C of the 320 K saturation level given by Kaufman *et al* (1990). However, because solar heated soil or dry grass in the tropics may be as hot as 43 °C, the next test required that the MIR brightness temperature had to be much greater than the TIR brightness temperature, indicative that the pixel contained a fire rather than a solar-heated surface. The third test checked that the pixel did not contain highly reflective cloud, which would also elevate the MIR brightness temperature relative to that in the TIR. Clouds are normally quite cold, so if the brightness temperature in the TIR was relatively high (more that –23 °C), then it probably did not contain cloud.

Setzer and Pereira (1991)

Also designed to detect forest burning in Brazil in AVHRR data, the method of Setzer and Pereira (1991) was somewhat more simple, involving a single test that used AVHRR channel 3 data, the pixel being flagged as hot if

$$T_{MIR} > 319 \text{ K}$$

Manual detection of smoke plumes with their source at the detected hot spot was then used to determine if the detection was real (i.e., associated with an active fire) or not (i.e., associated with solar heating). Another algorithm was published with a similar basis, but using DN criteria by Pereira and Setzer (1993). In this case, the pixel was flagged as hot if

$$DN < 10 \text{ or } 8$$

That is, if DN was close saturation, saturation in AVHRR theoretically being 0 (although see Electronic Supplement 1).

Brustet et al. (1991)

Designed to detect wild fires in West Africa using AVHRR (channel 3 and 4) data, the approach of Brustet *et al*. (1991) used scatter plots and frequency distributions of MIR versus TIR brightness temperatures to set thresholds on a case-by-case basis. As in the examples given in Figure 5.7 (for the scatter plot approach) and Figure 5.8 (for the histogram approach) of chapter 5, the scatter plots and histograms were used to define the cluster of values related to ambient surfaces, and outliers due to fires. The outliers could then be flagged as fire-containing pixels.

Kennedy et al. (1994)

Again designed to run on AVHRR data to detect wild fires burning in West Africa, the algorithm was essentially that of Kaufman *et al*. (1990), with a slightly higher T_{MIR} and ΔT threshold, plus an extra reflection test:

$$\begin{aligned} T_{MIR} &> 320 \text{ K} \\ \Delta T &> 15 \text{ K} \\ T_{TIR} &> 250 \text{ K} \\ R_{NIR} &< 16\ \% \end{aligned}$$

The final test used reflection in the NIR (AVHRR channel 2) to determine whether or not there were high levels of reflection. Presence of highly reflective surfaces could result in anomalously high T_{MIR} and ΔT, meaning that the pixel would pass the first two “hot tests” without necessarily containing a fire. This last test was thus designed to filter out such cases.

Chuvieco and Martin (1994)

Developed to detect forest fires in Spain using AVHRR data, the method of Chuvieco and Martin (1994) used a simple threshold applied to AVHRR channel 3 data to determine whether a pixel was hot or not:

$$\text{Day: } T_{MIR} > 317 \text{ K}$$
$$\text{Night: } T_{MIR} > 295 \text{ K}$$

The nighttime threshold level was reduced because the absence of reflection and solar heating by night meant that surface temperatures were lower. To avoid false detections due to solar heated soil, a forest mask was applied. This was obtained through "classification of several AVHRR normalized difference vegetation index (NDVI) images recorded prior to the fire", with the test only being applied to forest pixels, i.e., pixels within the forest mask.

Arino and Melinotte (1995)

The algorithm of Arino and Melinotte (1995) was designed to allow generation of a monthly atlas of fire index over Africa between July 1992 and June 1994. Developed at EAS/ESRIN, the algorithm ran on AVHRR data and involved five tests:

$$\begin{aligned} &T_{MIR} > 320 \text{ K} \\ &T_{MIR} > T_{TIR} + 15 \text{ (i.e., } \Delta T > 15 \text{ K)} \\ &T_{TIR} > 245 \text{ K} \\ &R_{VIS} < 25\,\% \\ &R_{VIS} - R_{NIR} > 1\,\% \end{aligned}$$

These are the tests of Kaufman *et al* (1990), as modified by Kennedy *et al*. (1994) and with the extra (reflection) test of Kennedy *et al*. (1994) added. However, also added was a fifth test that used reflection in AVHRR bands 1 and 2 R_{VIS} and R_{NIR} to check for sunglint, which could supply band 3 with unwanted levels of reflected radiance, hence allowing the T_{MIR} and ΔT tests to be passed.

Franca* et al. *(1995)

The final fixed threshold algorithm of the 1985–1995 period was published by Franca *et al*. (1995) to detect West African wild fires in AVHRR data. It involved five steps:

$$\begin{aligned} &T_{MIR} > 320 \text{ K} \\ &\Delta T > 15 \text{ K} \\ &T_{TIR} > 287 \text{ K} \\ &R_{VIS} < 9\,\% \\ &0 \le T_{10\mu m} - T_{12\mu m} \ge 5 \text{ K} \end{aligned}$$

$T_{10\mu m}$ and $T_{12\mu m}$ being the brightness temperature in AVHRR TIR channels 4 and 5.

The first four steps are now familiar, being the algorithm of Kaufman *et al* (1990), as modified by Kennedy *et al*. (1994), however, the final test was new. This test used the difference in temperature in AVHRR's 10 μm and 12 μm channels (i.e., channels 4 and 5) and checked that they were within the range 0 to 5 °C. This was a further cloud test, where in clear-sky conditions the $T_{10\mu m} - T_{12\mu m}$ difference is usually lower than 1 °C, although sometimes up to 2.5 °C. Thus, taking only pixels in this range meant that cloud-contaminated pixels were likely filtered out.

Contextual algorithms applied for fire detection: 1985–1995

While fixed threshold algorithms are quick to apply and require relatively little processing, contextual algorithms are a little more complex and require higher degrees of image processing. Four were applied for fire detection between 1985 and 1995, three being used with AVHRR data and one with GOES-VAS data. A further algorithm was used by NASA Goddard, as reported in the *IGBP-DIS Satellite Fire Detection Algorithm Workshop Technical Report* (Justice and Dowty, 1994), with a sixth algorithm being published in 1996. Generally such algorithms tended to use a 3 × 3 pixel kernel, such as that defined in Figure S8.1, to determine whether the central pixel in the kernel was anomalous when compared to the surrounding eight "background" pixels.

Flannigan and Vonder Haar (1986)

The first algorithm of the contextual type was that of Flannigan and Vonder Haar (1986). It was also the first algorithm to use ΔT. The algorithm, designed to detect forest fires in AVHRR data, followed four steps and applied four tests:

Step 1: Implement cloud-screening to mask and exclude cloud-contaminated pixels.

Step 2: Estimate the mean T_{MIR} and T_{TIR} for cloud-free background pixels from the eight pixels in a 9 × 9 pixel box centered on the target pixel (see Figure S8.1a).

Step 3: Locate fire-containing pixels by applying the following three tests:

Test (i) T_{MIR} of target pixel > mean T_{MIR} for the background

Test (ii) T_{TIR} of target pixel > mean T_{TIR} for the background

Test (ii) Target pixel ΔT > 8 K (nighttime) or ΔT > 10 K (daytime)

Pixels passing all three tests were flagged as fire-containing.

Step 4: Apply the two-component dual-band method, using the mean temperature estimated for the background pixels and the scan-angle-dependent pixel area, to estimate fire area and temperature (see Chapter 4).

By moving across the entire image, applying the same series of tests to each pixel in turn, the whole image could be checked for hot spots, with a different threshold being defined for each pixel depending on local background conditions.

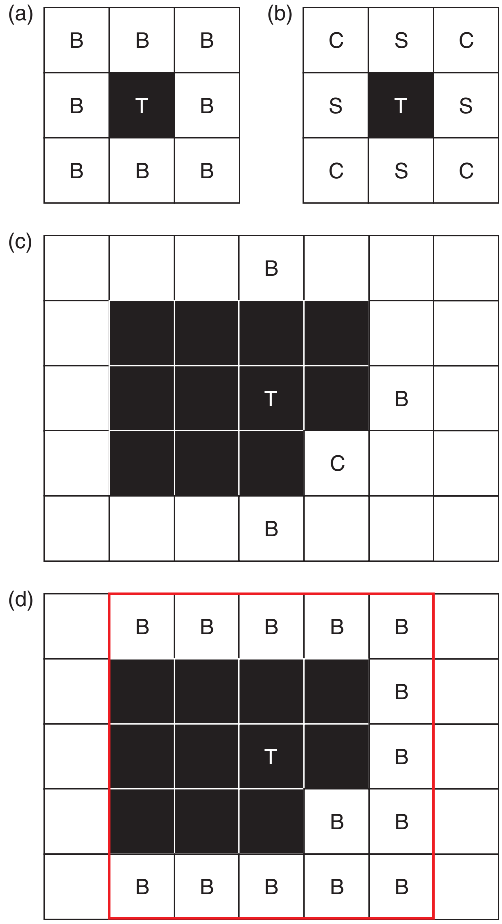

Figure S8.1 Kernel types used to apply contextual hot spot algorithms. In each case, the hot spot pixel(s) (black) are compared with statistics taken from the ambient background pixels (white). (a) Classic, where a 3 × 3 pixel box is centered on the hot target pixel (T), and background statistics are taken from the eight surrounding pixels (B). (b) Lee and Tag (1990) modification, whereby we distinguish between background pixels in the cardinal directions (side pixels: S) and corner pixels (C). (c) and (d) give solutions for cases whereby the target pixel is fully, or partially, surrounded by other hot spot pixels. (c) Langaas (1993) solution: whereby statistics are taken from the closest non-hot background pixels in the cardinal directions (B), or we can use the closest pixel (in this case corner pixel, C). (d) NASA/Goddard solution: whereby the size of the kernel is increased until at least 25 % of the background pixels are non-hot. In this case, this situation is reached for a 5 × 5 box centered on the target pixel (T). In this case, 11 of the 25 pixels in the kernel are hot, and 14 (56 %) are cold (valid) background pixels. Background statistics are now taken from those pixels marked B.

Lee and Tag (1990)

Designed to detect natural and anthropogenic fires in AVHRR data, Lee and Tag's (1990) approach was contextual in that it split each group of nine pixels into a target pixel, to be tested, and background pixels whose temperature statistics would be used to test for an anomaly in the central target pixel (see Figure S8.1b). However, rather than using the background pixels to set thresholds, it used their values to apply the dual-band method to the central pixel and assess whether the solution was compatible with the pixel containing a hot spot or not. The algorithm applied the following six steps:

Step 1: Apply a low temperature screen:
IF T_{TIR} for the target pixel < 263 K (−10 °C) THEN: Pixel is eliminated.
This acts as a crude cloud filter. Such a filter will need to be reduced in polar regions, at high altitudes, or over ice and snow covered terrain where surface temperatures (even anomaly temperatures) may be lower than –10 °C.

Step 2: Apply an atmospheric correction.
Lee and Tag (1990) used that of McClain *et al*. (1985) – see Electronic Supplement 4.

Step 3: Estimate the background temperature using the mean of the four atmospherically-corrected side pixels (side-pixel locations in relation to the target pixel are given in Figure S8.1b).

Step 4: Select a threshold hot component temperature (T_h) for a two component mixture model and use this, with the mean TIR background temperature obtained from the side pixels (= T_c), to estimate the size of the fire required to yield TIR pixel-integrated temperature for the target pixel, i.e., apply Equation 4.6c of Chapter 4:

$$p = \frac{M(\lambda, T_{\mathrm{int}}) - M(\lambda, T_c)}{M(\lambda, T_h) - M(\lambda, T_c)}$$

Step 5: Using the T_h and T_c input into the mixture model, with the output fire size, to estimate the corresponding pixel-integrated temperature in the MIR for the same two component mixture model, i.e., apply Equation 4.5 of Chapter 4:

$$\mathrm{M}(\lambda, \mathrm{T_{int}}) = \mathrm{M}(\lambda, \mathrm{T_h}) + (1–p)\,\mathrm{M}(\lambda, \mathrm{T}_c)$$

This value is then used as the threshold.

Step 6: If the T_{MIR} for target pixel is greater than the threshold, then pixel is flagged as a 'fire pixel'.

Execution of Step 4 requires assumption of a temperature for the hot component residing in the pixel. The range of hot component temperatures used by Lee and Tag (1990) to apply this model is given in Table S8.2. This tabulation shows that, although the incidence of false detection decreases with temperature selected for the hot component, so too does the number of hot spots located. We raise the issue here: is it better to detect all hot spots at the expense

Table S8.2. *Performance of the Lee and Tag (1990) contextual fire detection algorithm with increasing assumed hot spot temperature (in the dual-band model used to set fire size). Test was carried out by Lee and Tag (1990) on a 85 544 pixel image containing 20 hot spots [modified from Table 2 of Lee and Tag (1990)].*

Assumed fire temperature (K) (and in °C)	No. of hot spots correctly detected	% of hot spots detected	False detections
350 K (77 °C)	19	95	21
375 K (102 °C)	19	95	5
400 K (127 °C)	19	95	3
500 K (227 °C)	17	85	0
600 K (327 °C)	14	70	0

of many false detections, or to have no false detections, but not all of the hot spots? The answer to this question will depend in the objectives of the user (see Section 5.3.7 of Chapter 5).

ABBA (Prins and Menzel, 1994)

The Automated Biomass Burning Algorithm (ABBA) of Prins and Menzel (1994) was developed to detect seasonal variations in forest burning across South America in GOES-VAS data. Given the size of the region to be monitored, the number of fires to be located, the number of images available and duration of the study period (seasonal to annual), such an application required automation. The algorithm used elements of the Flannigan and Vonder Haar (1986) and Lee and Tag (1990) approaches to determine whether the pixel contained a hot spot or not. It also used regional statistics, rather than thresholds from local 9 × 9 pixel grids centered on each target pixel, to set image-dependent thresholds, an operation that reduces processing time. The algorithm followed seven steps and involved six tests:

Step 1: Implement a cloud-screen to mask and exclude cloud-contaminated pixels.

Step 2: Estimate the mean and standard deviation in T_{MIR} and T_{TIR} for all cloud-free pixels across a 150 km × 150 km sector. This defines the background values for each band ($T_{MIR\text{-}B}$ and $T_{TIR\text{-}B}$)

Step 3: Within that sector, execute the following two tests:

Test (i) ΔT for the target pixel > mean ΔT for the background.

Test (ii) T_{MIR} for the target pixel minus $T_{MIR\text{-}B} > 1.5 \times T_{MIR\text{-}B}$ standard deviation or 2 K (whichever is greater).

Pixels passing these tests are passed to the next step.

Step 4: Execute atmospheric, emissivity and reflection corrections to produce corrected values for each band ($T_{MIR\text{-}C}$ and $T_{TIR\text{-}C}$).

Step 5: Execute three more tests:
Test (iii) $T_{MIR\text{-}C} > 300$ K and $T_{TIR\text{-}C} > 295$ K.
Test (iv) $T_{TIR\text{-}C}$ for the target pixel minus $T_{TIR\text{-}C}$ for the background > 1 K.
Test (v) $T_{MIR\text{-}C}$ for the target pixel minus $T_{MIR\text{-}C}$ for the background > 5 K.
Pixels passing these tests are passed on to step 6.

Step 6: Apply the two-component dual-band method using the background temperature and scan-angle-dependent pixel area, to estimate fire area and temperature.

Step 7: Apply a final test:
Test (vi): Estimated fire temperature > 400 K.

This final test was applied to assess whether the dual-band solution was reasonable, and all pixels passing this final text were flagged as 'fire'.

We note that step 3 is designed to further reduce processing time by quickly eliminating pixels that almost certainly do not contain hot spots. The tests following step 3 then complete further checks to confirm, or reject, the presence of a fire in the remaining pixels.

Langaas (1993)

Building on the fixed threshold approach of Brustet *et al*. (1991), which used scatter plots of T_{MIR} versus T_{TIR} to set single band detection thresholds on an image-to-image basis, Langaas (1993) applied a semi-automated means by which the operator used the frequency distribution of temperatures, or digital numbers (DN), for an image (or sub-image) to assess an appropriate threshold. Like Lee and Tag (1990) and Prins and Menzel (1993), Langaas (1994) also assessed the output of the dual-band method to determine whether the result was reasonable, or not. The algorithm followed six steps and involved two tests:

Step 1: Divide the image into 'thermally homogeneous' sub-images.

Step 2: For each sub-image, produce a frequency distribution for DN or brightness temperature in the MIR. Use the distribution to assign a threshold value. Langaas (1993) did this on the basis of frequency, finding that the DN with a frequency of 50 was a suitable cut-off between fire pixels and non-fire pixels, so that this point was used to define the DN threshold. If, for example, the DN bin of 151 had a frequency of 50, then this was the threshold used for the sub-image case from which the histogram has been extracted.

Step 3: All pixels with a DN less than, or equal to, the threshold were flagged as potential fire pixels.
Note that the relation between radiance and DN is negative for AVHRR, so that lower DNs relate to higher pixel integrated temperatures; hence the requirement that DN needs to be less than, or equal to, the threshold. For sensors with a positive calibration, the test will be reversed: the appropriate frequency bin at the high end

of the distribution will be found and used to set a threshold, where all cases where DN $\geq$ the threshold will be defined as 'potential fire' pixels.

Step 4. Use the mean T_{TIR} of the four side pixels surrounding each potential fire pixel (or group of fire pixels) to define a background temperature (T_c).

Step 5: Use this background temperature to solve the two-component dual-band equation to output a fire temperature and size.

Step 6: Compare the extracted fire temperature with a threshold fire temperature to accept or reject the pixel: if the modeled temperature is greater than the chosen threshold fire temperature, then the pixel is a 'fire' pixel. A temperature of 470 K was selected by Langaas (1993) as an appropriate threshold for Savanna fires.

The algorithm of Langaas (1993) raises two new issues. First, the need to filter hot spots from the background of the target pixel so that it does not effect the 'ambient' threshold. Langaas (1993) achieved this by grouping his 'potential fire' pixels into 'agglomerates'. Then, for each target pixel within an agglomerate, he used the values from the nearest non-fire pixels in each of the cardinal directions, as shown in Figure S8.1c, to define the fire-free background. Second, if the TIR background temperature is greater than the T_{TIR} for the target pixel, then the dual-band method will not solve (see Chapter 4). In these cases, methods that rely on solution of the dual-band will fail and the fire will be missed. Langaas (1993) pointed out that this problem was not trivial, estimating that it caused 24 % of his fire pixels to be missed. For cases where $T_c \geq T_{TIR}$, Langaas (1993) used a modified background ($T_{c\text{-}m}$) calculated using:

$$T_{c\text{-}m} = T_{TIR\text{-}t} - T_{corr}$$

in which

$$T_{corr} = \frac{1}{n}\sum(T_{TIR-t} - T_{c-c})$$

Simply, the temperature of the target pixel ($T_{TIR\text{-}t}$) was reduced by a factor depending on the average of the difference between the target pixel and its background in each of the cardinal directions ($T_{c\text{-}c}$). This modified T_c was then used to solve the dual-band, it now being less than the T_{TIR} for the target pixel, thus allowing solution. It should be stressed that this correction should only be used to allow pixel detection, and not to extract meaningful solutions, it being very much a fabricated value: a value of convenience generated simply to allow the detection algorithm to function.

The NASA/Goddard (Justice and Dowty, 1994) approach

The problem of fire pixels existing in the background for the target pixel, and thereby corrupting the background-defined threshold, was further addressed by an algorithm developed at the NASA/Goddard Space Flight Center. The algorithm, developed for use with AVHRR data, was reported in Justice and Dowty (1994) and implemented two steps and four tests:

Step 1: Identify 'potential' fire pixels by completing the following three tests:

Test (i) Target pixel $T_{MIR} > 316$ K

Test (ii) Target pixel $T_{TIR} > 290$ K

Test (iii) Target pixel $T_{MIR} > T_{TIR}$ (i.e., $\Delta T >$ OK)

If the pixel passed all three tests, it was flagged as a 'potential' fire pixel. All operations now applied to just these pixels, reducing the number of pixels considered, and hence processing time.

Step 2: Complete a second level of tests on the 'potential' fire pixels:

Test (iv) Target pixel ΔT is greater than ΔT mean from the background, plus two times the standard deviation of the ΔT for the background pixels, or 3 K (whichever is greater).

Pixels passing this final test were classified as 'fire' pixels.

This was much like the Flannigan and Vonder Haar (1986) and ABBA algorithms, but calculated the mean and standard deviation for the background in a slightly more complex way, designed to exclude fire pixels from the calculation of the background statistics:

- A 3 × 3 pixel box was centered on the target pixel, and the background statistics were calculated using the eight pixels surrounding the central target pixel.
- However, background pixels that were also 'potential' fire pixels were excluded.
- Thus, the size of the background box was expanded, up to a maximum size of 21 × 21, until at least 25 % of the background pixels were 'non-fire' and thus available for calculation of the background statistics.
- There was a requirement that at least three pixels were available, otherwise the pixel was not classified.

A schematic showing this operation is given in Figure S8.1d.

Flasse and Ceccato (1996)

Flasse and Ceccato (1996) adopted a similar approach in developing their "*contextual algorithm for AVHRR fire detection*". The algorithm involved a pre-test, whereby 'potential' fire pixels were selected if:

(i) Target pixel $T_{MIR} > 311$ K, and

(ii) Target pixel $\Delta T > 8$ K

but rejected if

(iii) Target pixel $R_{NIR} \geq 20$ %

R_{NIR} being the reflection recorded in the near-infrared. As with the fixed threshold algorithms, rejection of pixels meeting the third condition reduced problems due to solar-heating and highly reflective surfaces (e.g., those experiencing sunglint). Finally, for each potential fire pixel, the following statistics were calculated:

$T_{MIR\text{-}b}$ = T_{MIR} mean for the potential fire pixel background;
$\sigma_{MIR\text{-}b}$ = T_{MIR} standard deviation for the potential fire pixel background;
ΔT_b = ΔT mean for the potential fire pixel background;
$\sigma_{\Delta Tb}$ = ΔT standard deviation for the potential fire pixel background.

Statistics were taken from a 3 × 3 window centered on the potential fire pixel, from which other potential fire pixels were excluded. The window was expanded to a maximum size of 15 × 15 pixels until the same criteria as the Justice and Dowty (1994) approach was achieved. Finally, the pixel was classified as a fire pixel if the following two tests were passed:

(iv) Target pixel T_{MIR} minus $[T_{MIR\text{-}b} - 2\sigma_{MIR\text{-}b}] > 3$ K

and

(v) Target pixel $\Delta T > [\Delta T_b - 2\sigma_{\Delta Tb}]$

Summation

This material is placed here to add detail to, and case-study support for, the generic hot spot detection models presented in Chapter 5. It is also the foundation on which most of the chapter 5 volcanic hot spot detection models are based. That is, they define and apply tests capable of determining whether a pixel is thermally anomalous in a spectral and/or spatial sense. The detail of fixed threshold algorithms applied for volcano hot spot detection, that could not be included in Chapter 5, are given in the following supplement (Electronic Supplement 9).

References

Al-Hinai, K. G. (1991). Oilfield fires of Kuwait. *International Journal of Remote Sensing*, **12**(12), 2447.
Arino, O. and Melinotte, J. M. (1995). Fire index atlas. *Earth Observation Quarterly*, **50**, 11–16.
Bakan, S., Chlond, A., Cubasch, U., Feichter, J., Graf, H., Grassl, H., Hasselmann, K., Kirchner, I., Latif, M., Roeckner, E., Sausen, R., Schlese, U., Schriever, D., Schult, I., Schumann, U., Sielmann, F. and Welke, W. (1991). Climate response to smoke from the burning oil wells in Kuwait. *Nature*, **351**, 367–371.
Brustet, J. M., Vickos, J. B., Fontain, J., Manissadjan, K., Podaire, A. and Lavenu, F. (1991). Remote sensing of biomass burning in West Africa with NOAA-AVHRR. In *Global Biomass Burning: atmospheric, climatic and bisopheric implications*, ed J. Levine, MIT Press, pp. 47–52.
Cracknell, A. P. (1997). *The Advanced Very High Resolution Radiometer*, London: Taylor & Francis, 534 p.
Dozier, J. (1980). Satellite identification of surface radiant temperature fields of subpixel resolution. *NOAA Technical Memorandum*, **NOAA-81021710**, Washington DC: National Earth Satellite Service, 17 p.

Chuvieco, E. and Martin, M. P. (1994). A simple method for fire growth mapping using AVHRR channel 3 data. *International Journal of Remote Sensing*, **15**(16), 3141–3146.

Flannigan, M. D. and Vonder Haar, T. H. (1986). Forest fire monitoring using NOAA satellite AVHRR. *Canadian Journal of Forest Research*, **16**, 975–982.

Flasse, S. P. and Ceccato, P. (1996). A contextual algorithm for AVHRR fire detection. *International Journal of Remote Sensing*, **17**(2), 419–424.

Franca, J.R.A., Brustet, J.-M. and Fontan, J. (1995). Multispectral remote sensing of biomass burning in West Africa. *Journal of Atmospheric Chemistry*, **22**, 81–110.

Justice, C. and Dowty, P. (1994). IGBP-DIS Satellite Fire Detection Algorithm Workshop Technical Report. *International Geosphere Biosphere Programme Working Paper*, **9**, Workshop held at NASA/GSFC, Greenbelt (MA), 25–26 February 1997, 88 p.

Kaufman, Y. J., Setzer, A., Justice, C., Tucker, C. J., Pereira, M. C. and Fung, I. (1990). Remote Sensing of biomass burning in the tropics. In *Fire in the tropical biota*, ed J. Goldhammer, Berlin: Springer-Verlag, pp. 371–399.

Kennedy, P. J., Belward, A. S. and Grégoire, J.-M. (1994). An improved approach to fire monitoring in West Africa using AVHRR data. *International Journal of Remote Sensing*, **15**(11), 2235–2255.

Khazenie, H. and Richardson, K. A. (1993). Detection of oil fire smoke over water in the Persian Gulf region. *Photogrammetric Engineering & Remote Sensing*, **59**(8), 1271–1276.

Langaas, S. (1993). A parametrised bispectral model for savanna fire detection using AVHRR night images. *International Journal of Remote Sensing*, **14**(12), 2245–2262.

Lee, T. F. and Tag, P. M. (1990). Improved detection of hotspots using the AVHRR 3.7 μm channel. *American Meteorological Society*, **71**(12), 1722–1730.

Paltridge, G. W. and Barber, J. (1988). Monitoring grassland dryness and fire potential in Australia with NOAA/AVHRR data. *Remote Sensing of Environment*, **25**, 381–394.

Pereira, M. C. and Setzer, A. W. (1993). Spectral characteristics of deforestation fires in NOAA/AVHRR images. *International Journal of Remote Sensing*, **14**(3), 583–597.

Prins, E. M. and Menzel, W. P. (1994). Trends in South American biomass burning detected with the GOES visible infrared spin scan radiometer atmospheric sounder from 1983–1991. *Journal of Geophysical Research*, **99**(D8), 16,719–16,735.

Prakash, A., Saraf, A. K., Gupta, R. P., Dutta, M. and Sundaram, R. M. (1995). Surface thermal anomalies associated with underground fires in Jharia coal mines, India. *International Journal of Remote Sensing*, **16**(12), 2105–2109.

Richter, R., Lehmann, F., Haydn, R. and Volk, P. (1986). Analysis of Landsat TM images of Chernobyl. *International Journal of Remote Sensing*, **7**(12), 1859–1867.

Rothery, D. A. (1989). A re-interpretation of Landsat TM data on Chernobyl. *International Journal of Remote Sensing*, **10**(8), 1423–1427.

Saraf, A. K., Prakash, A., Sengupta, S. and Gupta, R. P. (1995). Landsat-TM data for estimating ground temperature and depth of subsurface cola fire in the Jharia coalfield, India. *International Journal of Remote Sensing*, **16**(12), 2111–2124.

Setzer, A. W. and Pereira, M. C. (1991). Amazonia biomass burnings in 1987 and an estimate of their tropospheric emissions. *Ambio*, **20**(1), 19–22.

Stephens, G. and Matson, M. (1993). Monitoring the Persian Gulf war with NOAA AVHRR data. *International Journal of Remote Sensing*, **14**(7), 1423–1429.

Vidal, A., Pinglo, F., Durand, H., Devaux-Ros, C. and Maillet, A. (1994). Evaluation of a temporal fire risk index in the Mediterranean forests from NOAA thermal IR. *Remote Sensing of Environment*, **49**, 296–303.